Linear Multibeam Transmitarray Based on the Sliding Aperture Technique

Yuefeng Hou, *Student Member, IEEE*, Le Chang, *Student Member, IEEE*, Yue Li, *Senior Member, IEEE*, Zhijun Zhang, *Fellow, IEEE*, and Zhenghe Feng, *Fellow, IEEE*

***Abstract*— In the massive multiple-input multiple-output systems, the antennas should have the ability of beamforming. Under this requirement, the sliding aperture technique is adopted. In this paper, the principle of the sliding aperture technique is first demonstrated. This technique refers to the customization of each beam by part of the aperture, resulting in low scan loss over a wide angular range. Then, with the help of II-shaped transmit element, a linear multibeam transmitarray antenna based on the sliding aperture technique is designed. To the best of the authors' knowledge, the linear transmitarray is reported for the first time. The fabricated prototype shows that the proposed antenna can generate eight beams simultaneously covering the ±42° azimuth area with low scan loss and the beam intersection level better than −4 dB. The proposed antenna has been simulated, fabricated, and measured, and the experimental results are in good agreement with the simulation results.**

***Index Terms*— Beam selection, linear transmitarray, massive MIMO, multibeam, sliding aperture technique.**

I. Introduction

With the explosion of wireless mobile devices and services, some challenges, such as the spectrum crisis and high energy consumption, are emerging. To solve these problems, the fifth generation (5G) wireless communication systems have been popularly studied in many countries [1]. One of the promising key technologies in 5G is the massive MIMO due to the advantages in increasing data rates, energy efficiency, spectral efficiency, and mobility [2]. In the massive MIMO systems, base stations are equipped with a large number of antennas [3]. Antenna in a massive MIMO system should have the ability of beamforming, which means that wide beam-coverage domain with low scan loss is required.

To generate the required wide scanning angle, the active array antennas are the most straightforward solution [3]–[5]. With each active element integrated with a dedicated radio frequency (RF) chain, the antennas can realize high beam-steering resolution within wide scanning angle. At the same time, many efforts have been devoted to improve the active element performance or adding functionality [6]–[8]; for example, the magnetoelectric dipole antennas element with antiinterference characteristics [6], compact ultra-wideband multielement antennas with size reduction based on the simultaneous excitation of different characteristic modes [7], and the stacked patch elements integrated with the feeding network for higher gain and lower mutual coupling purposes [8]. However, the RF chain, including up/down converters, analog-to-digital converter, digital-to-analog converter, and so on, makes the whole massive MIMO system complex and expensive when the number of antenna elements is huge.

The principle of beam selection provides a new feasible solution for massive MIMO system. The concept of beam selection is to make the beam mapping first, and then merely select part of the beams [9]. Bam mapping is transforming the signals from antenna space into beam space. Meanwhile, recent researches have concluded that the beam-space MIMO can utilize beam selection to reduce the number of required RF chains in massive MIMO systems without obvious performance loss [10]–[14]. So, based on the principle of beam selection, beamforming can be simply realized by the multiple beams generated by passive networks. Moreover, for the purpose of meeting the communication requirement, the intersection level between the adjacent beams is preferred to be at most 3 dB lower than the maximum gain [15].

Under this requirement, in this paper, a linear multibeam transmitarray is proposed. The antenna has simple structure without feeding network. Based on the sliding aperture technique [16]–[19], the antenna has the advantages of wide beam-coverage domain with low scan loss. The proposed antenna in this paper is a symmetrical structure. It consists of a parallel plate waveguide, eight feed probes, and twenty phase-shifted elements. The antenna can generate eight fan-shaped beams simultaneously covering the ±42° azimuth area with above −4 dB point of intersection level between the adjacent beams which meets the requirement of the beam selection massive MIMO systems.

The remainder of the paper is organized as follows. The concept and design procedure of sliding aperture technique are presented in Section II. Section III describes the geometry of the proposed antenna, and the characteristics of parallel plate waveguide and phase-shifted elements are presented and discussed in detail. The manufactured prototype and its experimental performance are addressed in Section IV.

II. Principle of Sliding Aperture Technique

The schematic of the sliding aperture technique is illustrated in Fig. 1. The sliding aperture technique can realize multiple

Manuscript received January 9, 2017; revised February 26, 2018; accepted May 1, 2018. Date of publication May 11, 2018; date of current version August 2, 2018. This work was supported in part by the National Natural Science Foundation of China under Contract 61525104 and in part by the Beijing Natural Science Foundation under Contract 4182029. *(Corresponding author: Zhijun Zhang.)*

The authors are with the State Key Laboratory on Microwave and Communications, Tsinghua National Laboratory for Information Science and Technology, Tsinghua University, Beijing 100084, China (e-mail: zjzh@tsinghua.edu.cn).

Color versions of one or more of the figures in this paper are available online at http://ieeexplore.ieee.org.

Digital Object Identifier 10.1109/TAP.2018.2835506

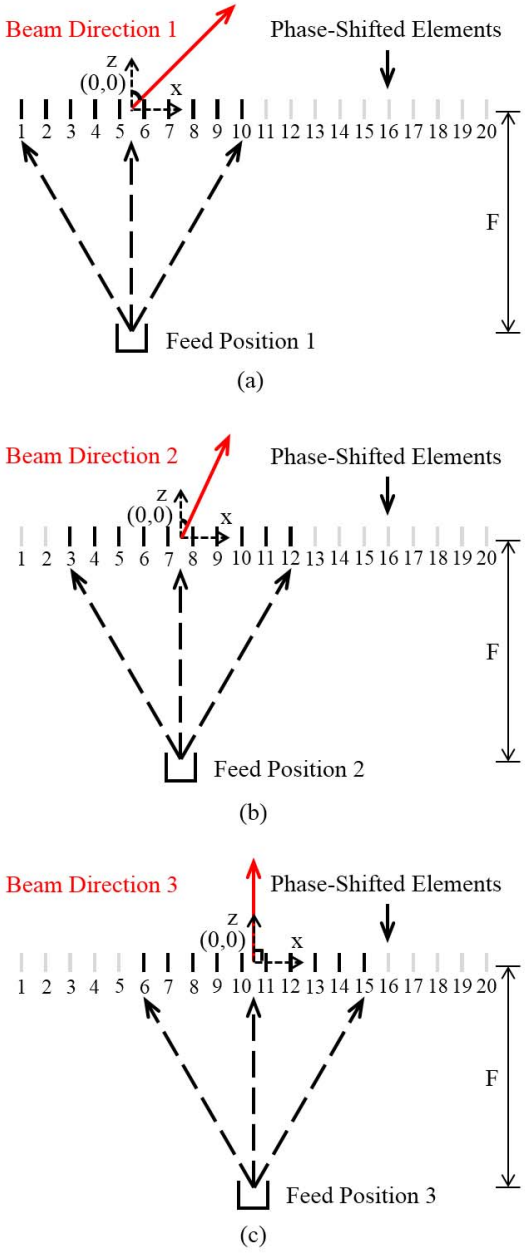

Fig. 1. Diagram of the sliding aperture technique: In the model, it is assumed that the phase distribution on the phase-shifted elements is axisymmetric, the minimum distance between phase center of the feed and elements are "F," the elements in black are illuminated by the feed, and the elements in gray are not illuminated by the feed. (a)–(c) Conditions when the feed sliding from left side to center of the array with the different transmitted beam directions.

beams with low scan loss over a wide angular range. For a transmitarray designed based on the sliding aperture technique, the feed can slide parallel to the phase-shifted array and the distance between the feed and the array keeps unchanged. Only parts of the array aperture can be illuminated at each feed position. No matter where the feed is, the compensation phase of the illuminated elements always satisfies the requirement of the specified beam directions.

The purpose of this section is to introduce the principle of the sliding aperture technique. The following example is not a real design process. To design a real array, a full-wave simulation software, as demonstrated in Section III, must be used. To simplify the model here, several assumptions are adopted.

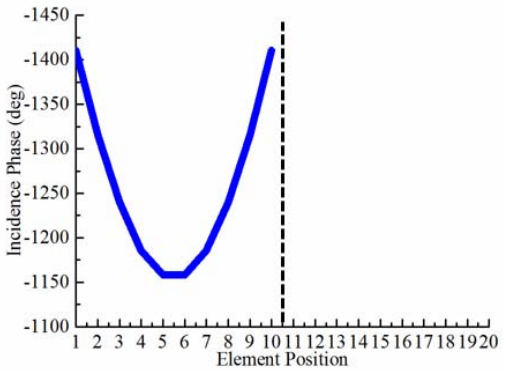

Fig. 2. Theoretical incidence phase in the left half of array based on the model with the "F" equals to 165.8 mm.

1) The model is a symmetrical transmitarray.
2) The model is in vacuum.
3) The vertical distance between the feed and the elements is "F."
4) The period of the elements is "P."
5) The number of the elements "n" is 20.
6) The mutual coupling effects are not considered in the model.
7) The middle of the illuminated elements is the origin point (0, 0).
8) The feed is assumed as a point source.
9) Located at the middle of the illuminated aperture, the feed radiates the energy perpendicular to the array, as shown in Fig. 1.
10) Because the feed in the actual design in Section III is a directional antenna, and the energy also reduces with the distance increasing, in this section, it is assumed that only half of the array aperture is illuminated at a time.

To make the description clearly and quantitatively, a model operating at 5.8 GHz is calculated using MATLAB

$$\varphi_{\text{incidence}} = -k_0 \times r_{mn} = -\frac{2 \times \pi \times f}{c} \times \sqrt{x_m^2 + F^2}. \quad \text{(I)}$$

For the illuminated element located at $(x_m, 0)$, the incidence phase of the element is calculated by formula (I). In the formula, the "f" is the working frequency of the model and the "c" is the speed of light. Formula (I) indicates that the incidence phase $\varphi_{\text{incidence}}$ of the element is determined by the phase constant k_0 and the distance between the feed and the element r_{mn}. Because the distance between the feed and the phase-shifted array is fixed, the incidence phase distributed on the illuminated array aperture is the same no matter where the feed is. Fig. 2 shows the incidence phase distribution when only the left of the array is illuminated by the feed

$$\varphi_{\text{transmitting}} = k_0 \times (n-1) \times P \times \sin\theta_0. \quad \text{(II)}$$

For the beam direction "θ_0," which is based on the requirement of designer, the transmitting phase $\varphi_{\text{transmitting}}$ is calculated by formula (II). Formula (II) indicates that the

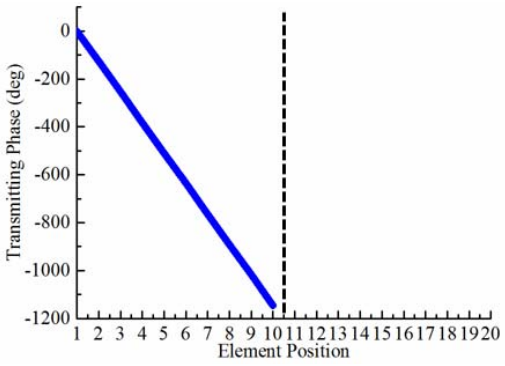

Fig. 3. Theoretical transmitting phase in the left half of array based on the model with the "F" equals to 165.8 mm.

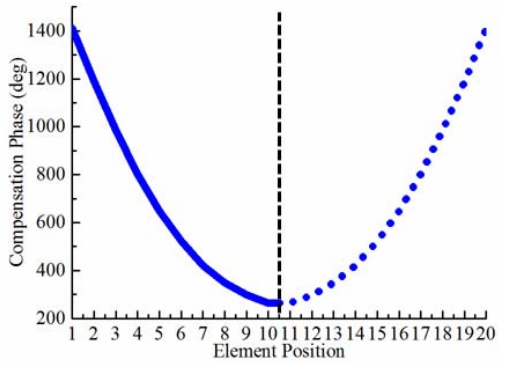

Fig. 4. Theoretical compensation phase of the all of array based on the model with the "F" equals to 165.8 mm. The compensation phase distribution of the array is symmetrical.

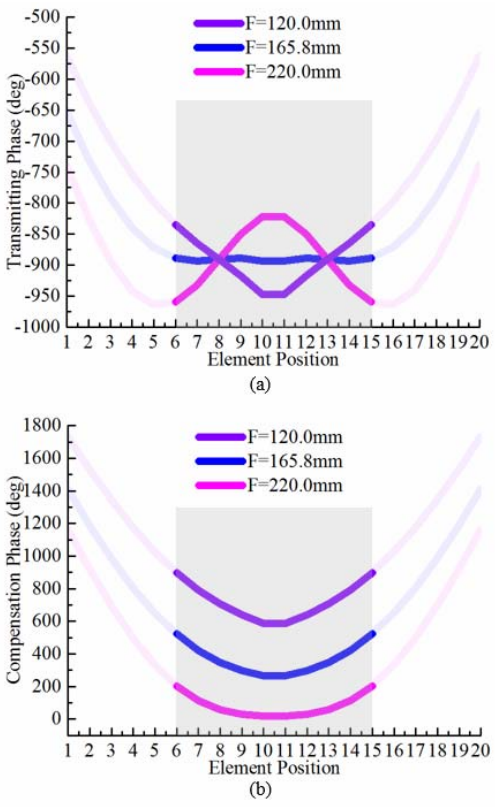

Fig. 5. Phase distribution in the middle half of the phase shifted array with different "F." (a) Transmitting phase distribution. (b) Compensation phase distribution. By chosen suitable "F," the transmitting phase value in the middle half of phase shifted array can be nearly equal to each other.

transmitting phase $\varphi_{\text{transmitting}}$ is determined by the phase constant "k_0," the number of the elements "n," the period of the elements "P," and the requirement beam direction "θ_0." When the scanning angle is $-45°$, the transmitting phase distribution in the left half of the array is shown in Fig. 3.

The compensation phase is the shifted phase of each element. It is equivalent to incidence phase subtracts from transmitting phase. Based on the calculated results shown in Figs. 2 and 3, the compensation phase distribution in the left half of array can be achieved. Because the array is symmetrical, the compensation phase of the right half can be obtained by mirroring, as shown in Fig. 4.

When the left half or right half of the array is illuminated by the feed, the transmitting direction is always $-45°$ or $45°$, respectively. However, if the compensation phase distribution in the middle part of the array is not considered in the design procedure, when the middle part of the array is illuminated by the feed, the compensation phase error can be significant.

So, in the next step, the distance "F" between the feed and the phase-shifted array is optimized to make the transmitarray realize a small compensation phase error in all scanning range. When changing the value of "F," the incidence phases on the elements are different, resulting in different compensation phase distributions, as shown in Fig. 5(a). The middle part of the array illuminated by the feed is the gray region. Because the design procedure is based on the maximal scanning angle in the beginning, it should be noted that the maximum beam direction can still be achieved for different compensation phase distribution shown in Fig. 5(a). For the middle half array, the compensation phase error is different under different values of "F." From Fig. 5(b), it is proved that when the middle of the array aperture is illuminated, an appropriate value of "F" can be found by optimization, and a nearly perfect transmitting phase distribution can be realized. As for the blue line in the gray region shown in Fig. 5(b), the maximum discrepancy is 4.6°.

After optimizing, the value of "F" is chosen to be 165.8 mm and the compensation phase distribution is also determined. When sliding the feed from left to the center of the array, the transmitting phases are shown in Fig. 6. The array illuminated by the feed is the gray region with blue line. From Fig. 6, the shifted phases of the illuminated elements are nearly a straight line and satisfy the requirement of the specified beam directions, which means little gain loss.

III. Linear Multibeam Transmitarray

Based on the requirement of beam selection, the antenna needs to generate multiple beams by passive feeding networks. One of the promising antennas is the Butler Matrix-based array. The Butler matrix is a special feeding network. When the different feed ports are excited, the feeding network can generate different phase gradients with the same magnitude, which indicates that the Butler matrix can generate multiple beams with low scan loss [20], [21]. Meanwhile, by modifying

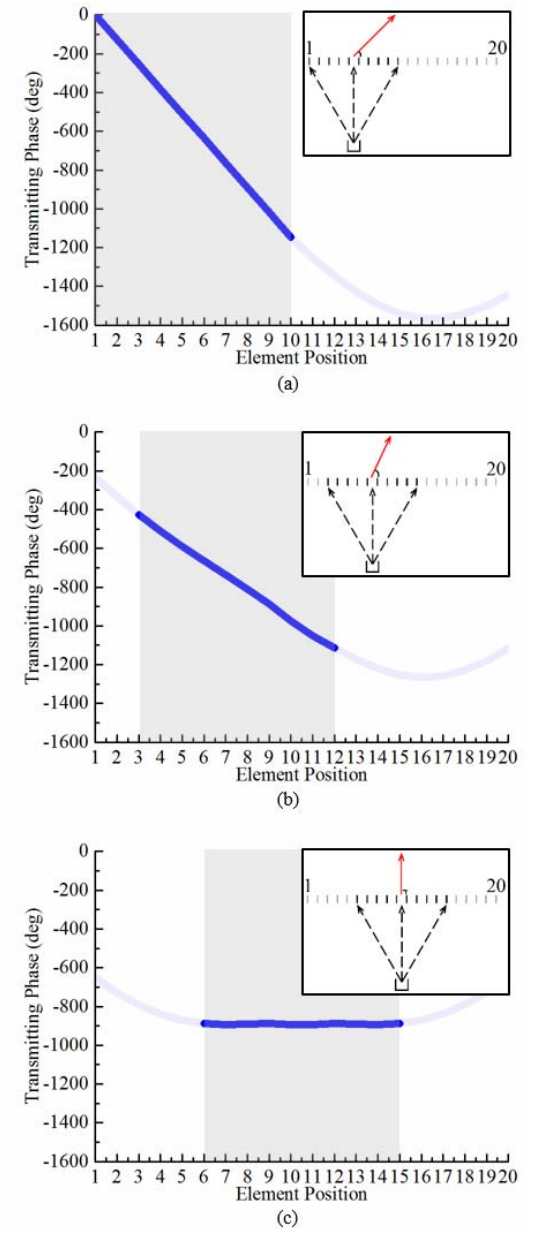

Fig. 6. Transmitting phase distribution. The blue line in the gray region is the transmitting phase of the elements illuminated by the feed. (a)–(c) Conditions when the feed sliding from left side to center of the array.

the structure of feeding network based on Butler matrix, special beam performance can be obtained by the antennas, such as 360° coverage over azimuth direction [15] and the coverage domain of beams defined arbitrarily within the uniformly distributed beams [22]. When the number of the feed ports increases, the Butler matrix-based array can generate more beams with different directions; however, the feeding network becomes complex and the dimension increase at the same time.

The lens antennas, such as grooved spherical lens [23] and flat lens [24], [25], have simple structure without feeding networks. The antennas mentioned above only have feeds and a phase-shifted array. Meanwhile, a novel technique of the energy radiated from the only part of the aperture that satisfies the compensation phase distribution is widely adopted in

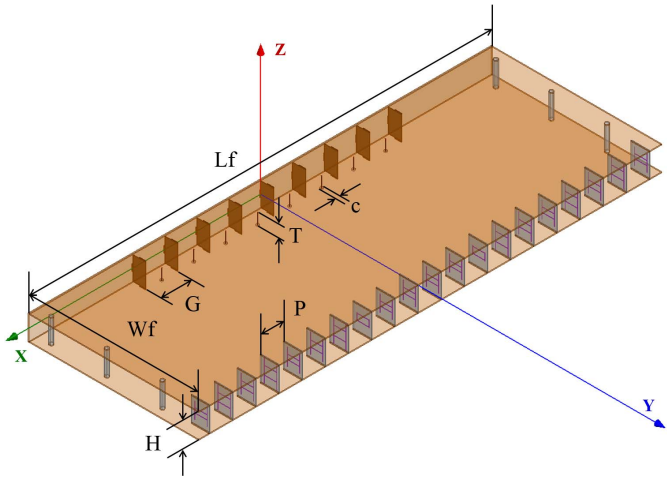

Fig. 7. Geometry of the linear multibeam transmitarray based on the sliding aperture technique.

TABLE I
PARAMETERS OF THE PARALLEL PLATE WAVEGUIDE

Parameters	Value
L	250 mm
W	183 mm
H	25 mm
G	34 mm
K	14 mm
r	14 mm
p	11 mm
d	0.8 mm

multiple designs, such as the shaped reflector hybrid antenna structure [16], the 500 m aperture spherical telescope [17], [18], and the mechanical beamsteering plate lens antenna [19]. Nevertheless, the antennas mentioned above mainly aim at realizing beam scanning with only one feed. Moreover, the aperture of the feeds mentioned in above literature is too large. When the mentioned feeds lined up to illuminate the phase-shifted array, the intersection angle is high and the intersection level between the adjacent beams is low. It indicates that the mentioned antennas do not satisfy the requirement of the beam selection massive MIMO systems.

Inspired by the principles and characteristics of the antennas mentioned above, in this paper, the structure of the proposed linear multibeam transmitarray is shown in Fig. 7. The antenna is composed of a parallel plate waveguide, eight feed probes and twenty phase-shifted elements. Next to each feed probe, there are two side metal walls and a metal back wall, which make up a backed cavity. To secure the top and bottom parts of the array, six nylon columns are added in the model. The nylon columns are located on the boundary of the antenna so that they have little influence on the performance of antenna. The parameters of the linear multibeam transmitarray are presented in Table I.

To apply the sliding aperture technique for the actual antenna design, several details are considered in this paper. First of all, by changing the dimension of the backed cavities and the position of the feed probes, the feeds are optimized to have a suitable width "G" of the aperture and realize a

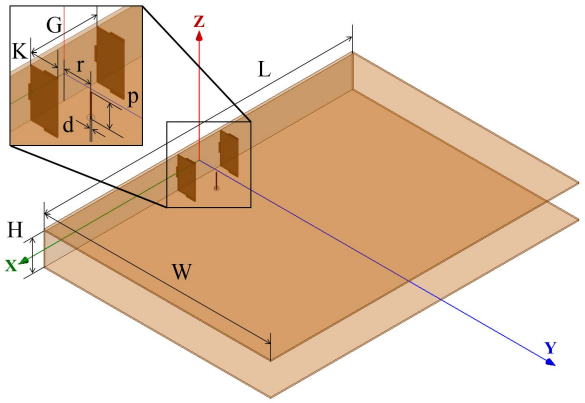

Fig. 8. Geometry of the parallel plate waveguide.

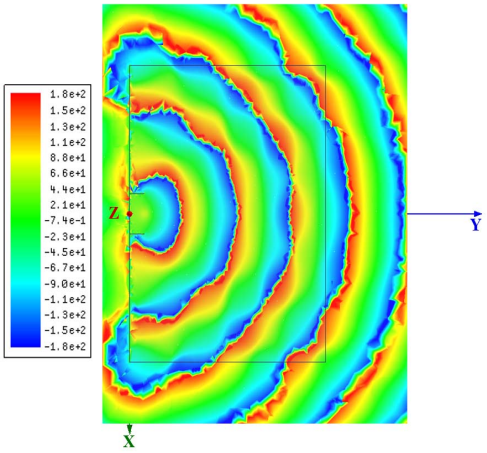

Fig. 9. Phase distribution on the *xoy* plane at the middle of the parallel plate waveguide.

suitable radiation pattern. Because the width "G" influences the separation between the adjacent beams, and radiation pattern influences the energy distribution on the elements. Furthermore, the tool of "Fields Calculator" in ANSYS HFSS software is applied in the simulation to ensure the incident phase distribution illuminated on the all of the elements extracted exactly. In addition, the elements are simulated in HFSS software with "Floquet Port" and "Master and Slave Boundary," which consider the mutual coupling effects between the elements.

Although the phase compensation distribution of the elements can realize beam steer from $-45°$ to $45°$, the antenna only generates eight beams covering the $\pm 42°$ azimuth area due to the limitation of the width "G" of the feed aperture. The antenna has been fabricated and tested, which will be described in Section IV. In order to analyze the key components of the proposed antenna clearly, the linear multibeam transmitarray is decomposed into a parallel plate waveguide and phase-shifted elements.

A. Design of Parallel Plate Waveguide

The configuration of the parallel plate waveguide is plotted in Fig. 8. The center frequency of the parallel plate waveguide is 5.8 GHz. It is fed by a feed probe with a backed cavity.

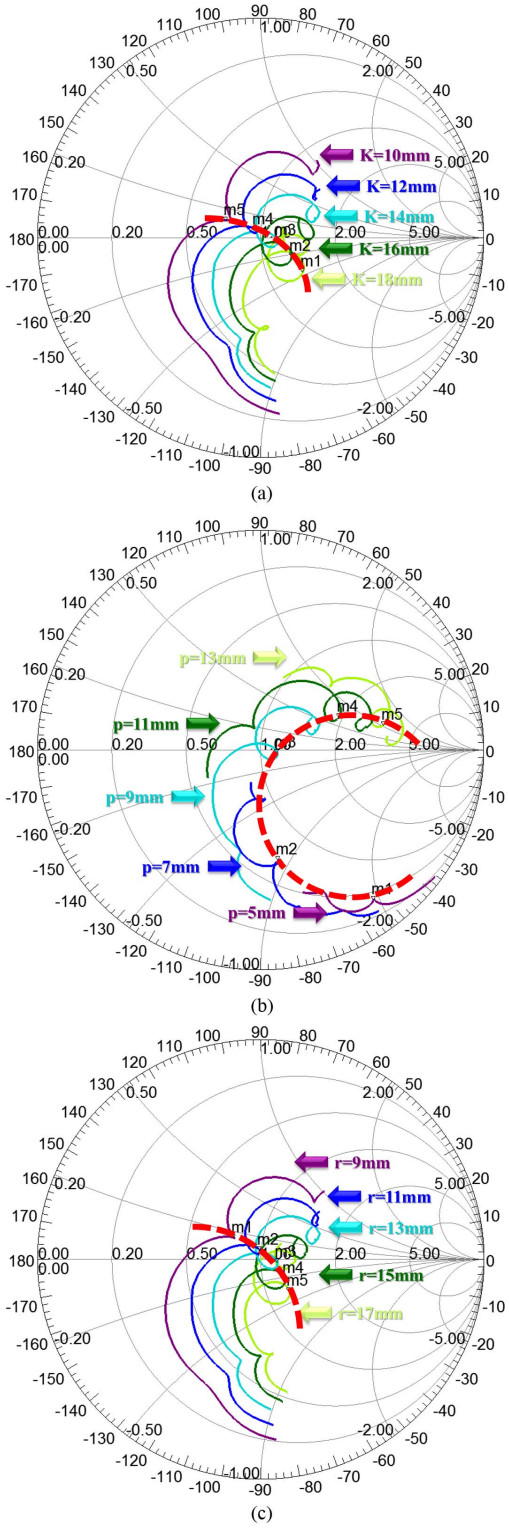

Fig. 10. Smith chart of the parallel plate waveguide with different parameters. (a) Length "K" of the back cavity. (b) Height "p" of the feed probe. (c) Distance "r" between the feed probe and metal back wall.

The parallel plate waveguide is adopted to propagate the TEM wave and restraints the energy in the linear space. Because the top plate and the bottom plate are metal, the E-field is vertical to the plates. To make the parallel plate

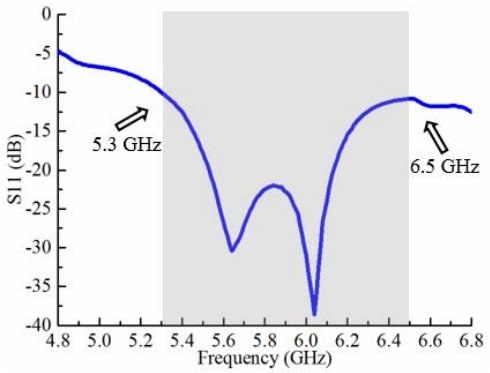

Fig. 11. Simulated reflection coefficients of the parallel plate waveguide.

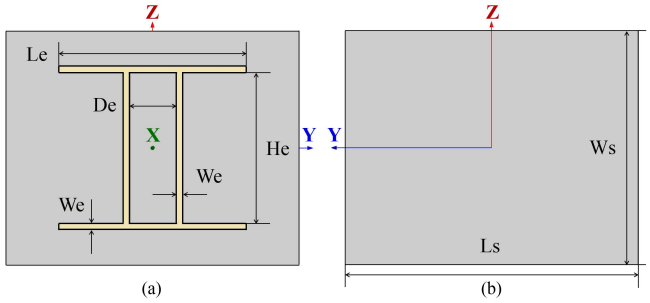

Fig. 12. Geometry of the phase-shifted elements. (a) Front view. (b) Back view.

waveguide operates in basic mode, the height "*H*" should not exceed half wavelength in the whole work frequency band. In the parallel plate waveguide, electromagnetic wave is spread in a fashion of cylindrical wave as shown in Fig. 9.

The length "*L*" of the parallel plate waveguide is determined by the number and period of elements, and the width "*W*" is the most important parameter to adjust the incidence phase distribution, similar to Fig. 5. The length "*G*" and the width "*W*" of the backed cavity, the distance "*r*" between the feed probes and metal back wall can be used to modify the energy distribution, which can enhance the aperture efficiency. The length "*p*" of the feed probes, the width "*W*," and the distance "*r*" have significant influence on the matching and bandwidth. The feed probe is a cylinder with diameter of "*d*."

To obtain a broad bandwidth, the parameters have been optimized elaborately. The curves changing by the parameters of "*K*," "*p*," and "*r*" on the smith chart are shown in Fig. 10. The lines of different colors indicate different values of the parameters. The marks on the curves present the real and imaginary parts position at center frequency. To bring out the tendency when varying the parameters, the marks are connected by dashed red line.

From Fig. 10(a), increasing the length "*K*," the performance of parallel plate waveguide is similar to add shunt capacitance. By changing the height "*p*," the position of marks varies obviously, which presents that the matching is significantly influenced by the height "*p*," as shown in Fig. 10(b). Meanwhile, the tendency is nearly orthogonal when changing the parameters of "*p*" and "*K*," which indicates that the parallel plate waveguide can be matched well by changing these parameters.

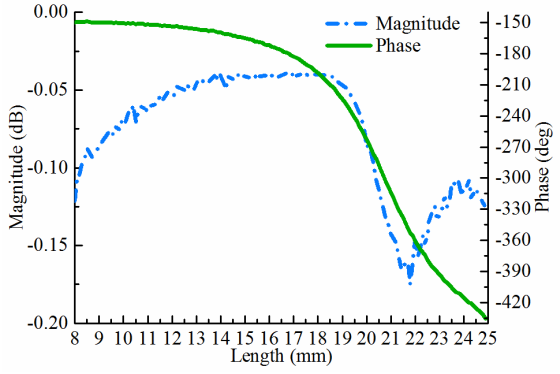

Fig. 13. Simulated transmission coefficients (magnitude and phase) of the proposed element versus the element dimension at 5.8 GHz.

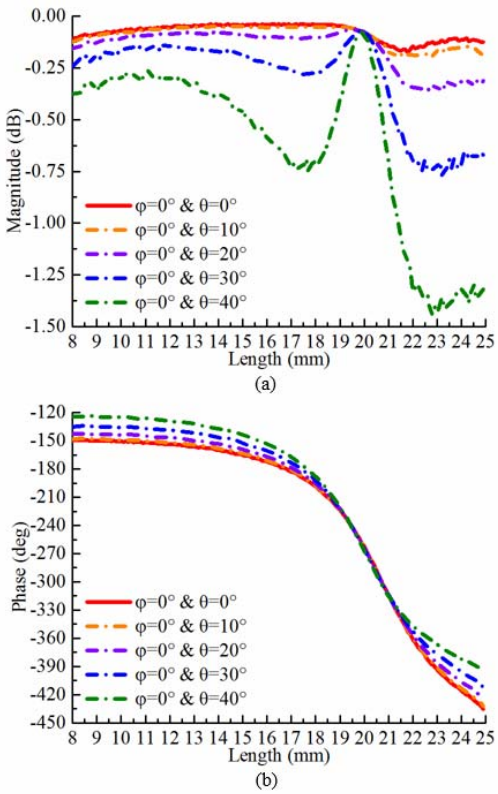

Fig. 14. Transmission performances at different oblique incidence angles versus length *L*. (a) Magnitude. (b) Phase.

The energy radiated from the feed probe in the parallel plate waveguide should not diverge excessively, otherwise radiation pattern will be worse. However, only varying the parameter of "*K*," it is conflicted with the energy distribution and bandwidth. To solve this problem, the distance "*r*" and the length "*K*" change simultaneously. From Fig. 10(c), when changing the distance "*r*," it has the similar tendency to the curves in Fig. 10(a). So, by adjusting the parameters of "*K*," "*p*," and "*r*," a broad bandwidth with suitable energy distribution can be obtained.

Then, by modifying the width "*W*," the compensation phase distribution can be determined, as descripted in Section II. After optimizing, the final parameters are shown in Table I, and

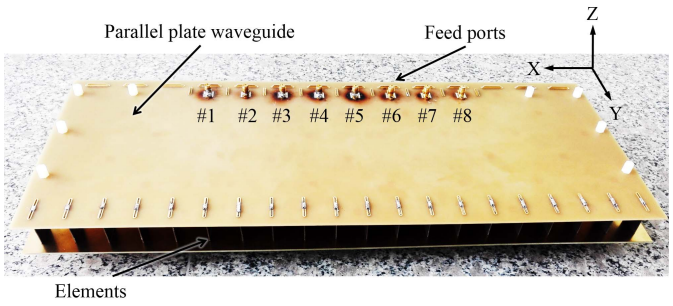

Fig. 15. Prototype of the proposed linear multibeam transmitarray antenna.

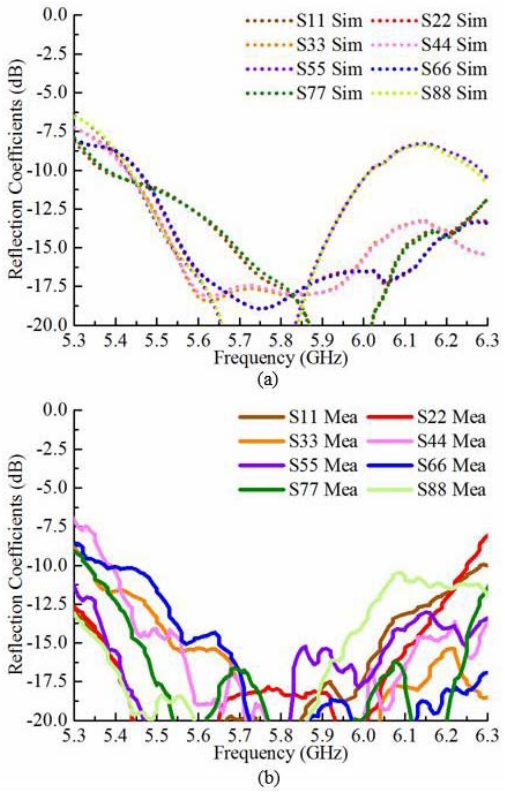

Fig. 16. Reflection coefficients of the feed ports from 1 to 8 with different colors. (a) Simulation results are shown as short dotted line. (b) Measured results are shown as solid line.

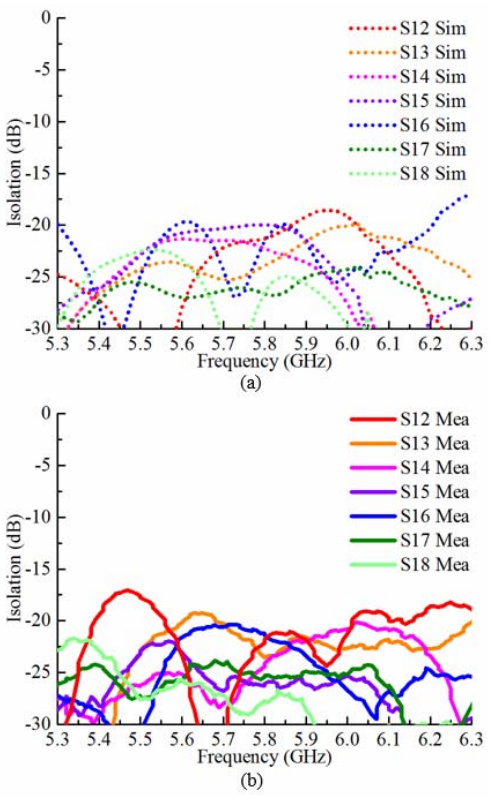

Fig. 17. Isolation parameter of the feed port 1 to the other feed ports. (a) Simulation results are shown as dotted line. (b) Measured results are shown as solid line.

the parallel plate waveguide with the parameters in Table I is simulated using HFSS software. The S11 of the parallel plate waveguide is shown in Fig. 11. The -10 dB bandwidth is 20.7% from 5.3 GHz to beyond 6.5 GHz, which indicates that the waveguide is suitable to be used as a space feed structure.

B. Design of Phase-Shifted Elements

The elements are designed based on one-layered metalens element [26]. To simplify the design of elements, the element is printed on one side of a PCB. As shown in Fig. 12, the structure with yellow color represents the metal and the background with gray color represents the substrate. The geometry and dimension of the element are illustrated in Fig. 12. The height "Hs" and the width "Ws" of the substrate is 4 and 5 mm, respectively. The substrate has the thickness "Ss" of 0.79 mm and the relative permittivity of 2.2 and $\tan\delta = 0.0009$ (Taconic TLY dielectric). The element has two stubstrips parallel to the y-axis and stubstrips connected by two strips parallel to the z-axis. The strips are with the width "We" of 1 mm. The distance "He" of two stubstrips parallel to the y-axis is 5 mm. The two stubstrips parallel to the z-axis are arranged symmetrically from the center with a distance of $\mathrm{De} = 23 \times \mathrm{Le}^2 - 0.68 \times \mathrm{Le} + 8.65$ mm. "Le" is used to tune the phase relation. The distance "P" between the two elements parallel to the x-axis is 6 mm.

The elements are simulated in the HFSS software by the "Floquet Ports" and "Master and Slave boundary," which considers the mutual coupling between the elements. In simulation, the incident wave and transmitted wave are with linear polarization parallel to the y-axis and the direction of propagation is parallel to the z-axis. The magnitude and phase of transmission coefficients with different arm lengths from 8 to 25 mm at 5.8 GHz are shown in Fig. 13. The blue curve shows that the magnitude is better than -0.2 dB. For the phase response, shown as the green curve, a wide range of 286° is achieved, which satisfies the phase compensation range of the parallel plate waveguide.

Fig. 14 depicts the variations in the transmission magnitude and phase at different oblique incidence angles. The parameters φ and θ are the azimuth and elevation angles of the incidence wave, respectively. Because the elements position are changing along the x-axis, the different oblique incidence angles θ are analyzed while keeping the angle $\varphi = 0°$.

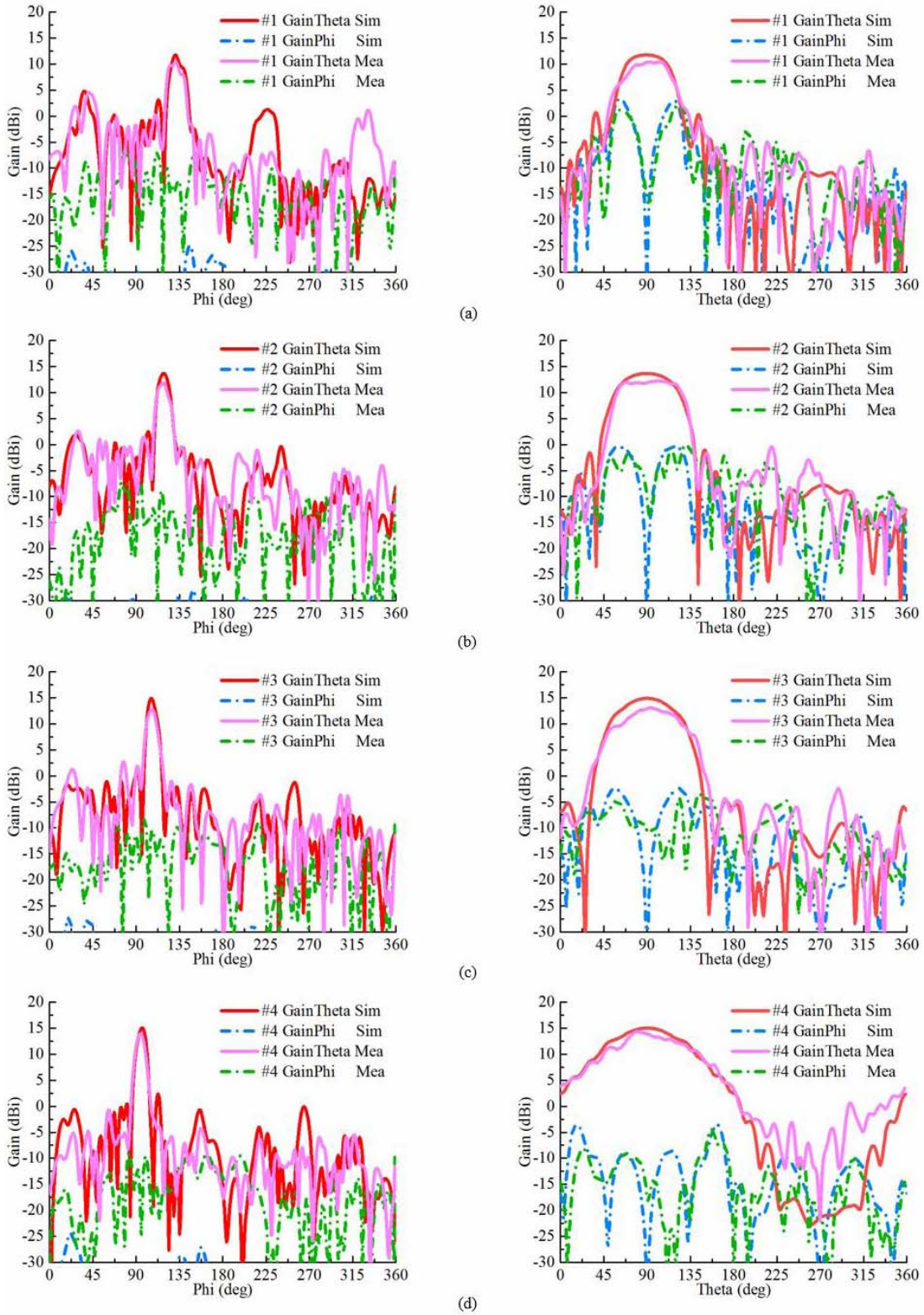

Fig. 18. Radiation patterns of H-plane and E-plane at 5.8 GHz. (a) Feed port 1. (b) Feed port 2. (c) Feed port 3. (d) Feed port 4. The number of feed ports and the coordinate system of the radiation patterns refer to Figs. 7 or 15. The radiation patterns in H-plane are shown as short dash-dotted line and the radiation patterns in E-plane are shown as solid line.

With the changes in different oblique incident angles θ, the transmit magnitude is shown in Fig. 14(a). When the θ is less than 30°, the transmit magnitude is better than -1 dB. Fig. 14(b) shows the phase at different oblique incidence angles. The phases nearly have the same rate of curving with the same range of phase shifted, which indicates that the phase compensation will be stable when used in the parallel plate waveguide to generate different direction beams.

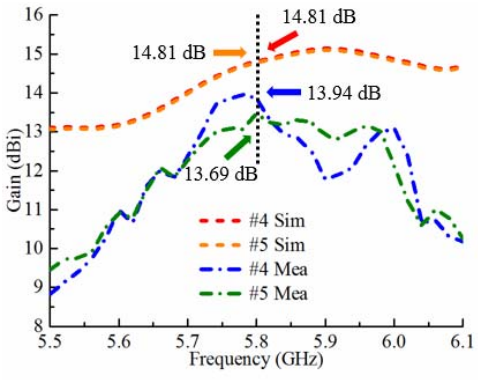

Fig. 19. Simulated and measured bore-sight gain of the proposed antenna with port four and port five.

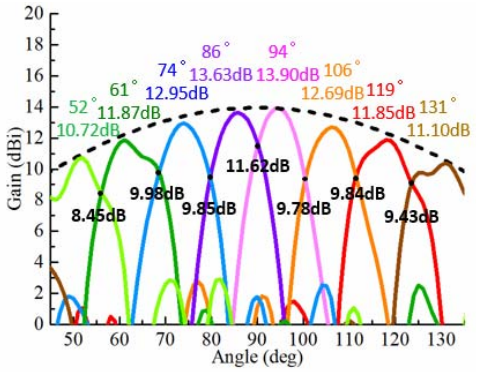

Fig. 20. Radiation pattern of the proposed antenna with eight ports at 5.75 GHz. The maximum gain in H-plane and the direction of each beam are shown above the beams and the color is the same as the curves of the corresponding beams. At the crossing position of the adjacent two beams, the gain is shown using the black color.

IV. Simulation and Measurement Results

The proposed linear multibeam transmitarray is fabricated and measured, and the prototype is shown in Fig. 15. The prototype has the same dimension and structure as the model shown in Fig. 7, and the detailed dimension of the prototype is presented in Table I. The parallel plate waveguide of the prototype is made by the substrate of FR4 with a thickness of 1 mm. The plane of the substrate, which is the internal face of the parallel plate waveguide, is covered by metal. Eight cavities consisted by one feed probe and three metal walls are inserted on one narrow side of the parallel plate waveguide. The metal walls are made by the substrate of FR4 with all the planes covered by metal. Twenty elements are inserted from the slots on the other narrow side of the parallel plate waveguide. The elements have the same structure as the model shown in Fig. 12, and the period of the elements is the same as the "P." The dimension of the elements is different with the different transmission phases and high transmission magnitude, as shown in Fig. 13. The compensation phase distribution of the elements is based on sliding aperture technique, which is presented in Section II. When the eight feeds sliding from one side to the other side, eight beams covering the $\pm 42°$ azimuth area with low scan loss are obtained in turn, and the point of intersection between the adjacent beams is above -4 dB.

The simulated and measured reflection coefficients are shown in Fig. 16. The measured results are performed by a N5071B vector network analyzer (300 KHz–9 GHz). The result shows that the eight ports are matched well and the -10 dB impedance bandwidths of all the ports are more than 26%. The isolation is shown in Fig. 17. As an example, the isolation of port one is compared and all isolation are lower than -15 dB, which means good isolation.

Because the antenna has a structure symmetrical about y-axis, when the symmetrical feed ports illuminate the energy, the radiation patterns and directions of the two beams are symmetrical by the y-axis with approximately the same gain in the results of simulation and measurement. The radiation patterns of the feed ports 1–4 are shown in Fig. 18. The E-plane of the radiation pattern is cut in the yoz plane and the H-plane of the radiation pattern is cut in the xoy plane. The feed ports 1 is the far left of all ports as shown in Fig. 15. With the number of the feed port increase, the position of the feed port is close to center. Fig. 18(a) shows the H-plane and E-plane radiation patterns of the port one, and fan-shaped beam is generated. The H-plane radiation pattern is slightly distorted due to the performance deterioration of the phase-shifted element when the incidence angle is too big. When the port position is close to the center, the beamwidth is wider in E-plane and narrower in H-plane with a higher gain. From Fig. 15, the antenna has the characteristics of low cross polarization. The gain of the measured results is slightly lower than the simulation result less than 1.7 dB in the center of the radiation pattern. The tolerance is mainly because of the weld and fabricate error.

In Fig. 19, the maximum gain of the ports four and five in simulation and measurement is compared. The gain difference between the simulation and measurement at 5.8 GHz is less than 0.9 and 1.15 dB, respectively. From Fig. 15, the middle of the antenna is slightly curving due to fabricated error. The maximum gain of the measurement result is not in the xoy plane. The measured H-plane patterns are shown in Fig. 20. The maximum gain and the direction of each beam are marked in Fig. 20. Form Fig. 20, the gain of each beam represents a $\cos\theta$ distribution, which indicates that the phase compensation of the elements has a little phase error based on the sliding aperture technique.

V. Conclusion

In this paper, a linear multibeam transmitarray antenna is designed. The concept and design procedure of the sliding aperture technique are described in detail. By combining the novel structure and design principle, the antenna can obtain eight beams covering the $\pm 42°$ azimuth area with low scan loss and the beam overlapped level is better than -4 dB. The measured results show a good agreement with the simulation.

References

[1] S. Chen and J. Zhao, "The requirements, challenges, and technologies for 5G of terrestrial mobile telecommunication," *IEEE Commun. Mag.*, vol. 52, no. 5, pp. 36–43, May 2014.

[2] E. G. Larsson, O. Edfors, F. Tufvesson, and T. L. Marzetta, "Massive MIMO for next generation wireless systems," *IEEE Commun. Mag.*, vol. 52, no. 2, pp. 186–195, Feb. 2014.
[3] P. Xingdong, H. Wei, Y. Tianyang, and L. Linsheng, "Design and implementation of an active multibeam antenna system with 64 RF channels and 256 antenna elements for massive MIMO application in 5G wireless communications," *China Commun.*, vol. 11, no. 11, pp. 16–23, Nov. 2014.
[4] W. Roh *et al.*, "Millimeter-wave beamforming as an enabling technology for 5G cellular communications: Theoretical feasibility and prototype results," *IEEE Commun. Mag.*, vol. 52, no. 2, pp. 106–113, Feb. 2014.
[5] L. Li, W. Hong, Y. Zhang, Z. Chen, and P. Chen, "Design and implementation of an active array antenna with remote controllable radiation patterns for mobile communications," *IEEE Trans. Antennas Propag.*, vol. 62, no. 2, pp. 913–921, Feb. 2014.
[6] H. Zhai, J. Zhang, Y. Zang, Q. Gao, and C. Liang, "An LTE base-station magnetoelectric dipole antenna with anti-interference characteristics and its MIMO system application," *IEEE Antennas Wireless Propag. Lett.*, vol. 14, pp. 906–909, 2015.
[7] D. Manteuffel and R. Martens, "Compact multimode multielement antenna for indoor UWB massive MIMO," *IEEE Trans. Antennas Propag.*, vol. 64, no. 7, pp. 2689–2697, Jul. 2016.
[8] Y. Gao, R. Ma, Y. Wang, Q. Zhang, and C. Parini, "Stacked patch antenna with dual-polarization and low mutual coupling for massive MIMO," *IEEE Trans. Antennas Propag.*, vol. 64, no. 10, pp. 4544–4549, Oct. 2016.
[9] J. Brady, N. Behdad, and A. M. Sayeed, "Beamspace MIMO for millimeter-wave communications: System architecture, modeling, analysis, and measurements," *IEEE Trans. Antennas Propag.*, vol. 61, no. 7, pp. 3814–3827, Jul. 2013.
[10] W. Choi, A. Forenza, J. G. Andrews, and R. W. Heath, Jr., "Opportunistic space-division multiple access with beam selection," *IEEE Trans. Commun.*, vol. 55, no. 12, pp. 2371–2380, Dec. 2007.
[11] J. Choi, "Beam selection in mm-wave multiuser MIMO systems using compressive sensing," *IEEE Trans. Commun.*, vol. 63, no. 8, pp. 2936–2947, Aug. 2015.
[12] P. V. Amadori and C. Masouros, "Low RF-complexity millimeter-wave beamspace-MIMO systems by beam selection," *IEEE Trans. Commun.*, vol. 63, no. 6, pp. 2212–2223, Jun. 2015.
[13] X. Gao, L. Dai, Z. Chen, Z. Wang, and Z. Zhang, "Near-optimal beam selection for beamspace mmWave massive MIMO systems," *IEEE Commun. Lett.*, vol. 20, no. 5, pp. 1054–1057, May 2016.
[14] X. Jiang, H. Wang, Z. Zhang, X. Gao, L. Dai, and M. F. Iskander, "Low RF-complexity massive MIMO systems based on vertical spatial filtering for urban macro cellular networks," *IEEE Trans. Veh. Technol.*, vol. 66, no. 10, pp. 9214–9225, Oct. 2017.
[15] P. Chen *et al.*, "A multibeam antenna based on substrate integrated waveguide technology for MIMO wireless communications," *IEEE Trans. Antennas Propag.*, vol. 57, no. 6, pp. 1813–1821, Jun. 2009.
[16] Y. B. Jung and S. O. Park, "Ka-band shaped reflector hybrid antenna illuminated by microstrip-fed horn array," *IEEE Trans. Antennas Propag.*, vol. 56, no. 12, pp. 3863–3867, Dec. 2008.
[17] B. Peng *et al.*, "Preparatory study for constructing fast, the world's largest single dish," *Proc. IEEE*, vol. 97, no. 8, pp. 1391–1402, Aug. 2009.
[18] B. Dong and J. L. Han, "Beam patterns and wideband feed for the five-hundred-meter aperture spherical telescope," in *Proc. URSI GASS*, Beijing, China, Aug. 2014, pp. 1–4.
[19] E. B. Lima, S. A. Matos, J. R. Costa, C. A. Fernandes, and N. J. G. Fonseca, "Circular polarization wide-angle beam steering at Ka-band by in-plane translation of a plate lens antenna," *IEEE Trans. Antennas Propag.*, vol. 63, no. 12, pp. 5443–5455, Dec. 2015.
[20] J. Butler and R. Lowe, "Beam-forming matrix simplifies design of electronically scanned antennas," *Electron. Des.*, vol. 12, pp. 170–173, Sep. 1961.
[21] P. Liu, Z. Zhang, Y. Li, and Z. Feng, "A dual-beam eight-element antenna array with compact CPWG crossover structure," *IEEE Antennas Wireless Propag. Lett.*, vol. 16, pp. 1269–1272, 2017.
[22] H.-T. Chou, "An effective design procedure of multibeam phased array antennas for the applications of multisatellite/coverage communications," *IEEE Trans. Antennas Propag.*, vol. 64, no. 10, pp. 4218–4227, Oct. 2016.
[23] Z. Briqech, A.-R. Sebak, and T. A. Denidni, "Wide-scan MSC-AFTSA array-fed grooved spherical lens antenna for millimeter-wave MIMO applications," *IEEE Trans. Antennas Propag.*, vol. 64, no. 7, pp. 2971–2980, Jul. 2016.
[24] S. B. Yeap, X. Qing, and Z. N. Chen, "77-GHz dual-layer transmitarray for automotive radar applications," *IEEE Trans. Antennas Propag.*, vol. 63, no. 6, pp. 2833–2837, Jun. 2015.
[25] M. Li, M. A. Al-Joumayly, and N. Behdad, "Broadband true-time-delay microwave lenses based on miniaturized element frequency selective surfaces," *IEEE Trans. Antennas Propag.*, vol. 61, no. 3, pp. 1166–1179, Mar. 2013.
[26] Y. Hou, Y. Li, Z. Zhang, and Z. Feng, "Dual-layered metalens for polarization-agile orbital angular momentum wave," in *Proc. ISAPE*, Guilin, China, Oct. 2016, pp. 546–549.

Yuefeng Hou (S'16) received the B.S. degree from the University of Electronic Science and Technology of China, Chengdu, China, in 2015. He is currently pursuing the Ph.D. degree in electrical engineering with Tsinghua University, Beijing, China.

His current research interests include leaky-wave endfire antenna arrays, reduced massive MIMO antenna arrays, and metamaterials.

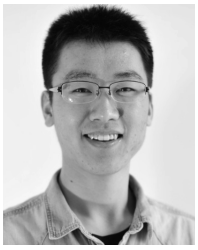

Le Chang (S'16) received the B.S. degree in electronics and information engineering from Xidian University, Xi'an, China, in 2012, and the Ph.D. degree in electrical engineering from Tsinghua University, Beijing, China, in 2017.

He is currently a Senior Engineer with Huawei Device Ltd., Beijing.

Yue Li (S'11–M'12–SM'17) received the B.S. degree in telecommunication engineering from Zhejiang University, Zhejiang, China, in 2007, and the Ph.D. degree in electronic engineering from Tsinghua University, Beijing, China, in 2012.

In 2012, he was a Post-doctoral Fellow with the Department of Electronic Engineering, Tsinghua University. In 2013, he was a Research Scholar with the Department of Electrical and Systems Engineering, University of Pennsylvania, Philadelphia, PA, USA. He was also a Visiting Scholar with the Institute for Infocomm Research (I2R), A∗STAR, Singapore, in 2010, and the Hawaii Center of Advanced Communication, University of Hawaii at Manoa, Honolulu, HI, USA, in 2012. Since 2016, he has been with Tsinghua University, where he is an Associate Professor with the Department of Electronic Engineering. He has authored or co-authored over 90 journal papers and 30 international conference papers, and holds 15 Chinese patents. His current research interests include metamaterials, plasmonics, electromagnetics, nanocircuits, mobile and handset antennas, MIMO and diversity antennas, and millimeter-wave antennas and arrays.

Dr. Li was a recipient of the Issac Koga Gold Medal from URSI General Assembly in 2017, the Second Prize of Science and Technology Award of China Institute of Communications in 2017, the Best Student Paper Award (3rd prize) form APCAP 2017, the Young Scientist Award from URSI AP-RASC 2016, the Young Scientist Award from EMTS 2016, the Best Student Paper Award form ICMMT 2016, the Best Paper Award form ISAPE 2016, the Young Scientist Award from URSI General Assembly in 2014, the Outstanding Doctoral Dissertation of Beijing Municipality in 2013, and the Principal Scholarship of Tsinghua University in 2011. He was the Associate Editor of the IEEE TRANSACTIONS ON ANTENNAS AND PROPAGATION and the IEEE ANTENNAS AND WIRELESS PROPAGATION LETTERS.

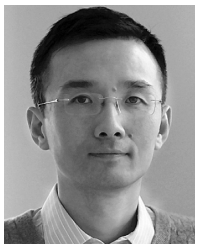

Zhijun Zhang (M'00–SM'04–F'15) received the B.S. and M.S. degrees from the University of Electronic Science and Technology of China, Chengdu, China, in 1992 and 1995, respectively, and the Ph.D. degree from Tsinghua University, Beijing, China, in 1999.

In 1999, he was a Post-Doctoral Fellow with the Department of Electrical Engineering, University of Utah, Salt Lake City, UT, USA, where he was a Research Assistant Professor, in 2001. In 2002, he was an Assistant Researcher with the University of Hawaii at Manoa, Honolulu, HI, USA. In 2002, he joined Amphenol T&M Antennas, Vernon Hills, IL, USA, as a Senior Staff Antenna Development Engineer and was then promoted to the position of Antenna Engineer Manager. In 2004, he joined Nokia Inc., San Diego, CA, USA, as a Senior Antenna Design Engineer. In 2006, he joined Apple Inc., Cupertino, CA, as a Senior Antenna Design Engineer and was then promoted to the position of Principal Antenna Engineer. Since 2007, he has been with Tsinghua University, where he is currently a Professor with the Department of Electronic Engineering. He has authored the book *Antenna Design for Mobile Devices* (Wiley, 1st edition 2011, 2nd edition 2017).

Dr. Zhang was an Associate Editor of the IEEE TRANSACTIONS ON ANTENNAS AND PROPAGATION from 2010 to 2014 and the IEEE ANTENNAS AND WIRELESS PROPAGATION LETTERS from 2009 to 2015.

Zhenghe Feng (M'05–SM'08–F'12) received the B.S. degree in radio and electronics from Tsinghua University, Beijing, China, in 1970.

Since 1970, he has been with Tsinghua University, as an Assistant, Lecturer, Associate Professor, and Full Professor. His current research interests include numerical techniques and computational electromagnetics, RF and microwave circuits and antennas, wireless communications, smart antennas, and spatial temporal signal processing.